Science and Technology Journal Vol. 12 Issue: 2 June 2024 ISSN: 2321-3388

Synthesis, Characterization, Photoluminescence and Photocatalytic Properties of Pr(III) Doped $CdMoO_4$ Phosphors

N. Mohondas Singh[1*], K. Lalchhandama[2], Fidelia Lalrindiki[3], and Brojendro Singh Shagolsem[4]

[1,2,3,4]Department of Chemistry, School of Physical Sciences,
Mizoram University, Aizawl-796004, India
*E-Mail: nmdas08@rediffmail.com
[*]Corresponding Author

Abstract—In this study, tetragonal-shaped $CdMoO_4:Pr^{3+}$ phosphors were produced using the co-precipitation approach at room temperature. The sample was characterised using various methods such as UV-visible spectroscopy, FT-IR, SEM, and XRD. XRD pattern revealed a tetragonal phase, and FT-IR spectroscopy indicated that the sample had adsorbed H_2O molecules. SEM studies showed the aggregation and development of irregular shapes in the prepared samples. Excitation spectra were obtained by setting the λ_{em} wavelength at 605 nm, which resulted in the detection of strong peaks at transitions of ($^3H_4 \rightarrow {}^3P_2$), ($^3H_4 \rightarrow {}^3P_1$), and ($^3H_4 \rightarrow {}^3P_0$) at 453 nm, 477 nm, and 495 nm respectively. Emission spectra were also obtained by exciting the Pr^{3+} ions at 468 nm, resulting in the detection of distinctive emission spectra at 561 nm and 654 nm at a transition of ($^3P_0 \rightarrow {}^3H_5$) and ($^3P_0 \rightarrow {}^3F_2$), with a degradation percentage of 95.063% successfully obtained. Using Tauc's plot, the band-gap energy was calculated, and the band-gap energy was found to be 4.415 eV, deemed suitable for photocatalytic activity. The decay curves were well-fitted using the bi-exponential equation for the prepared sample, obtaining an R^2 value of 0.977, indicating that the process follows first-order kinetics.

Keywords: $CdMoO_4$: Pr^{3+}, XRD, photocatalytic, Kinetic study, PL Spectroscopy, decay curve

INTRODUCTION

Rare earth-activated inorganic phosphors are becoming more and more common in lighting and display technologies, including cathode ray tubes, field emission displays, plasma display panels, and many other optical devices; research on these materials has increased significantly in recent years (Lin *et al.* 2014). These materials are made of a host lattice and an activator ion. The activator ion, a dopant rare earth ion, acts as an activator and emits radiation (Lin *et al*. 2016). On the other hand, the parity-forbidden f-f transitions of rare earth ions resulted in poor cross-sections and luminescence efficiency (Nedeljkovic *et al*. 2013). Therefore, it is necessary to include them in an appropriate host matrix to boost the luminescence intensity, stability, and colour purity, among other things.

Due to their outstanding thermal, chemical, hardness, and physical stability, metal molybdates with scheelite structures are considered decent hosts for luminescent materials. Due to its exceptional optical and chemical properties, the molybdate compounds $CdMoO_4$, isostructural to $CaMoO_4$, and $PbMoO_4$ are among the most intriguing. It formed a tetragonal crystal structure with a $C^{4h}{}_6$ space group and an orthorhombic unit cell as the body centre. This compound might be a promising option for a luminescent material because of its significant thermal and chemical stabilities and remarkable crystallographic anisotropy (Wang *et al.* 2013). The roughly tetrahedral symmetry of each Mo^{6+} in the tetragonal structure of $CdMoO_4$ is encircled by four equivalent oxygen sites, while

https://doi.org/10.22232/stj.2024.12.02.02

each Cd^{2+} is coordinated to eight oxygen sites. It is well known that annealing temperature and doping ion concentrations significantly impact a phosphor's photoluminescence property. $CdMoO_4$ has been synthesised using various techniques, such as hydrothermal, reverse micelle, co-precipitation, and others. However, because it is so inexpensive, the high emission efficiency synthesis at room temperature is especially attractive. At room temperature, red luminescence $CdMoO_4:Eu^{3+}$ was synthesised by Wang and his workers (Chen *et al*. 2012).

Additionally, a report on the photoluminescence characteristics of the sonically synthesised $CdMoO_4:Ln^{3+}$ (Ln = Dy, Sm, Eu, Pr, Ho, and Er) (Gan *et al*. 2014). According to the author's expertise, no studies have been done on the impact of dopant ion concentration on the behaviour of photoluminescence of $CdMoO_4:Pr^{3+}$ and its photocatalytic activity. Therefore, the current work's main objective is to investigate the photoluminescence behaviour of $CdMoO_4$ that has been synthesised at room temperature and doped with various Pr^{3+} concentrations.

EXPERIMENTAL SECTION

Sample Preparation

$Cd(NO_3)_2{\cdot}4H_2O$(LOBACHEMIEPVT.LTD),$(NH_4)_6Mo_7O_{24}{\cdot}4H_2O$, (SDFCL), and $PrCl_3{\cdot}xH_2O$ (99.9%, Alfa-Aesar) were used in the co-precipitation method at room temperature to create the phosphors $CdMoO_4:Pr^{3+}$. Stoichiometric volumes of $Cd(NO_3)_2$ and $PrCl_3$ were dissolved in 25 millilitres of double-distilled water for this synthesis procedure. Then, drop by drop, with constant magnetic stirring, the separately produced $(NH_4)_6Mo_7O_{24}{\cdot}4H_2O$ solution was added to the aforementioned solution. Five hours of magnetic stirring were spent on the combined solution. The mixture was then refrigerated without being shaken or stirred for five days. Centrifugation was used to separate the white precipitates, which were then cleaned five times using double distilled water and acetone. The precipitates were dried for 24 hours at 70°C in an oven (Singh *et al*. 2018).

Characterization of the Sample

The UV-visible absorbance spectrum and degradation studies of the sample were obtained using the UV-visible spectrophotometer EVOLUTION 220. To determine their absorption band, the prepared sample was sent to FT-IR Spectroscopy (SHIMADZU CORP - 00703). Utilising powder X-ray diffraction (XRD - BRUNKER AXS, D8 FOCUS-Powder) investigation, the phase and chemical composition of the $CdMoO_4:Pr^{3+}$ phosphor were ascertained. The photoluminescence property of the sample was evaluated using the Fluorescence Spectrophotometer (F-7000). The morphology and particle size of the samples were analysed using SEM (JOEL-JSM-6390LV).

RESULTS AND DISCUSSION

XRD Study

The $CdMoO_4$ tetragonal structure, as reported by JCPDS no. 07-0209, has cell characteristics of a = b = 5.155, c = 11.194, and V = 297.473 is shown by XRD analyses in Fig.1. The tetragonal phase of $CdMoO_4$ may be properly indexed, to every one of the observed diffraction peaks. We increase the reactant concentration, $[Cd^{2+}]=[MoO_4^{2-}]$ = 0.02 M to $[Cd^{2+}] = [MoO_4^{2-}]$ = 0.14 M, throughout this time to track the impact of reactant concentration on size and morphology. The highest intensity of the 2θ Degree of 29.217 corresponds to the (112) body centred of the tetragonal system of $CdMoO_4$, while the lowest intensity, having (332) planes lies at 2θ of 80.918. Fig. 1 demonstrates that the majority of the as-obtained products are large-scale microspheres, suggesting that a high yield may be achieved under the chosen reaction conditions. We observed that the product can maintain its spherical form with a change in reactant concentration. By careful inspection, it can be seen that the reactant concentration significantly influences the monodispersity and homogeneity of $CdMoO_4$ microspheres. Fine morphology is not favoured by reactant concentrations that are either too high or too low. To synthesise, it is crucial to select an ideal situation ($[Cd^{2+}] = [MoO_4^{2-}]$ = 0.10 M). $CdMoO_4$ has a limited size distribution, perfect spherical form, and less aggregating (Singh *et al*. 2018).

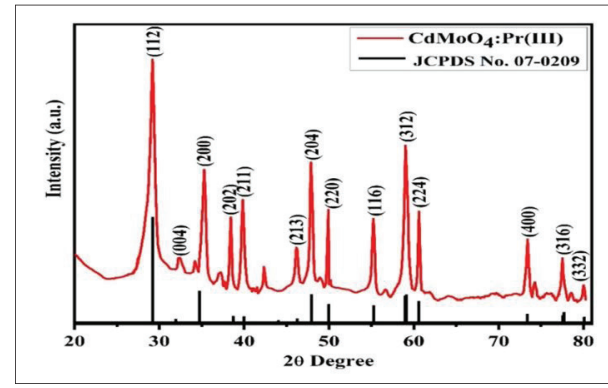

Fig. 1: XRD Patterns of $CdMoO_4:Pr^{3+}$.

FT-IR and SEM Study

The $CdMoO_4$ sample was subjected to FT-IR spectroscopy, as shown in Fig. 2. There are observations of the bands at 455.20, 540.07, 817.82, 833.25, 1491, and 2487cm^{-1}. Mo-O and Cd-O bending vibration has been implicated due to the absorption band at 455.20 and 540.07 cm^{-1}. O-Mo-O lengths of the MoO_4 tetrahedron are associated with a prominent absorption band at 817.82 and 833.25 cm^{-1}. This suggests that the as-prepared particles have formed the crystalline $CdMoO_4$ phase. The absorption band identifies the CO_2 on the sample's surface with a centre at 2487 cm^{-1}. The water-bending vibration of O-H deposited on the samples' surface is responsible for the absorption band at 1491 cm^{-1}. Since the samples were created in aqueous solutions, absorbed water molecules will inevitability end up on the surface of the particles (Wang *et al*. 2013).

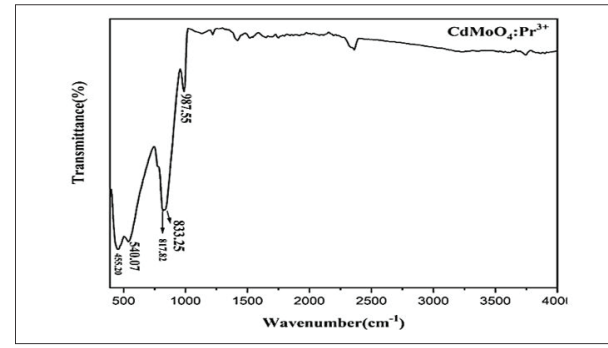

Fig. 2: FT-IR Spectra of $CdMoO_4:Pr^{3+}$.

Small particles are made up of several irregular nanoparticles (NPs), according to a high-magnification SEM image. We discovered that the sources of Mo and Cd are essential for developing the microsphere structures. The average particle size was calculated and found to be 70.5 nm (Varela *et al.* 2011).

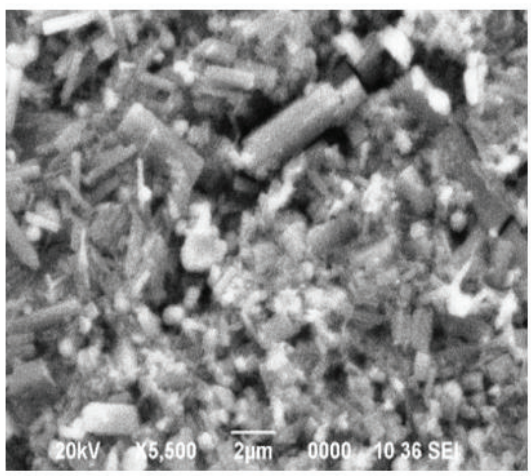

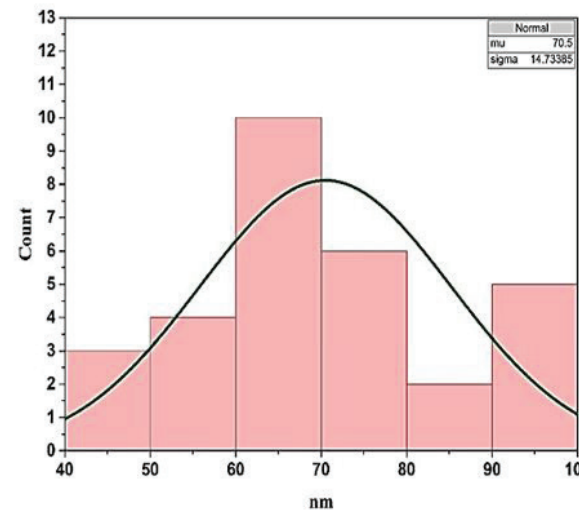

Fig. 3: SEM Image of $CdMoO_4:Pr^{3+}$ an Average Particle Size (70.5 nm).

Optical Property Study

The sample absorption peak was speculated to be around 209.860 nm, within a wavelength range of 190 to 280 nm, due to O-Mo charge transfer transitions (CTT) of MoO_4^{2-} groups. The spectral profile was steep, indicating that the band-gap transition rather than the transition from the impurity level was responsible for the absorption (Wang *et al*. 2014). The band-gap was determined for $CdMoO_4:Pr^{3+}$ using Tauc's plot, and the semiconductor's band-gap energy may be derived by using the following equation:

$$\alpha h\nu = A(h\nu - Eg)^n$$

The energy intercept plot of $(\alpha h\nu)^2(eVcm^{-1})^2$ versus energy is plotted which yields the E_g for a direct transition. By this method, the band gap energy for the $CdWO_4:Pr^{3+}$ sample is found to be 4.415 eV (Wang *et al*. 2014).

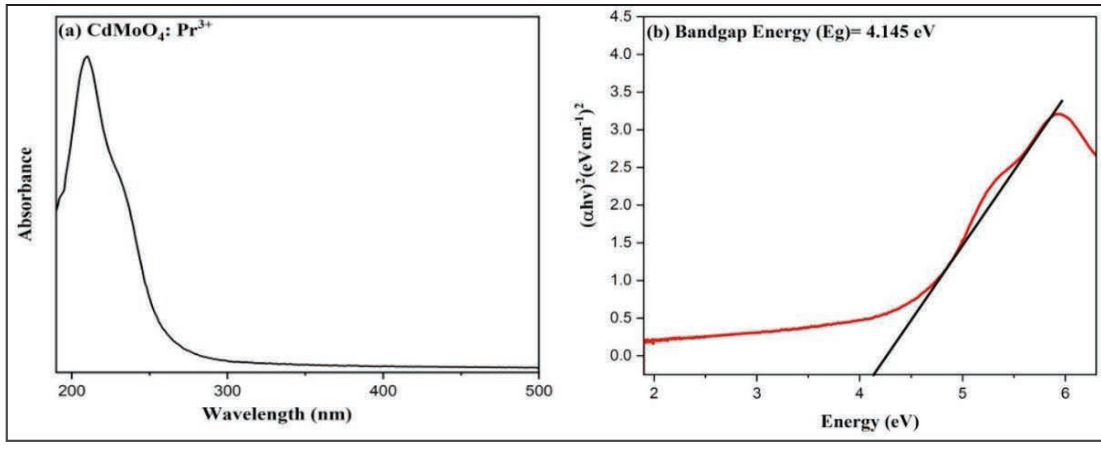

Fig. 4: (a) UV Spectra of $CdMoO_4:Pr^{3+}$; (b) Bandgap Energy Value of $CdMoO_4:Pr^{3+}$.

PL Study

At room temperature, the $CdMoO_4:Pr^{3+}$ phosphor's excitation and emission spectra are displayed in Figures 5a and 5b. The excitation spectra measured at 605 nm have a broadband that can be identified, with a maximum of 322 nm. This band originates from the charge transfer bands (CTB) between the molybdate core atom and oxygen ligands inside MoO_4^{2-} groups. Some of the sharp lines, as shown in Fig. 5a, have long wavelengths: 453 nm ($^3H_4 \rightarrow {}^3P_2$), 477 nm ($^3H_4 \rightarrow {}^3P_1$), and 495 nm ($^3H_4 \rightarrow {}^3P_0$), respectively. These lines are located between 400 and 500 nm in wavelength [33]. Zhang and colleagues have shown that excitation into the MoO_4^{2-} group at 322 nm produces the characteristic emission spectra of the Pr^{3+} ions at 561 nm ($^3P_0 \rightarrow {}^3H_5$) and 654 nm ($^3P_0 \rightarrow {}^3F_2$) (Sun *et al.* 2011).

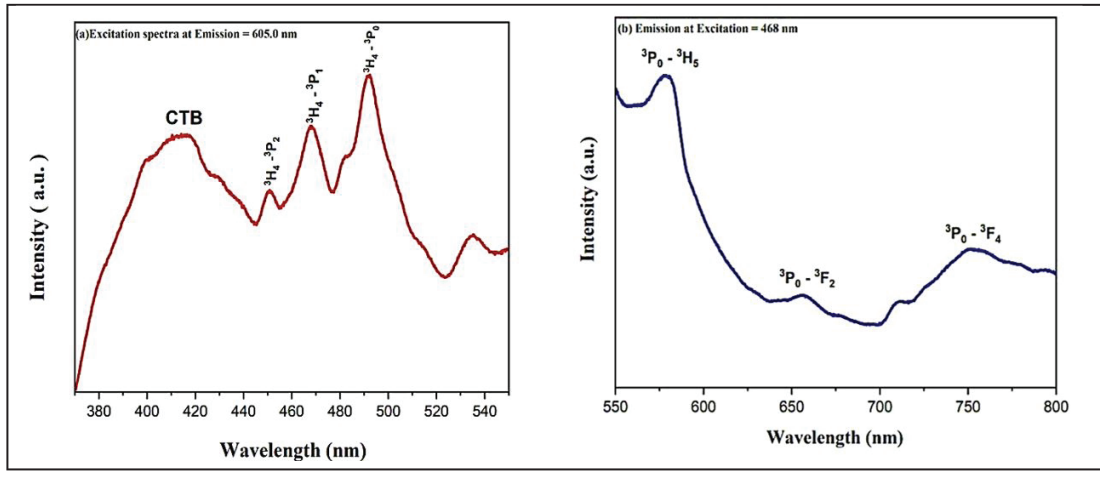

Fig. 5: (a) PL Spectra of Pr^{3+} Doped $CdMoO_4$ λ_{em}=605 nm; (b) PL Spectra of Pr^{3+} Doped $CdMoO_4$ λ_{ex}=468 nm.

CIE Analysis

For photoluminescence applications, a phosphor's CIE colour coordinates are crucial. Based on the emission spectra data seen when stimulated at 335 nm, Fig. 6 displays the CIE chromaticity diagram for samples of $CdMoO_4:Pr^{3+}$(5 at. %) that have been synthesised and stored at room temperature. The predicted colour coordinates (x, y) for the $CdMoO_4:Pr^{3+}$(5 at. %) samples as produced and at room temperature are determined to be (0.255, 0.212), respectively. From this plot, it can be seen that all samples are displayed in the bluish-purple colour area, and the inset

in this image depicts the emission colour seen upon UV light excitation at 468 nm (Nongmaithem *et al*. 2014).

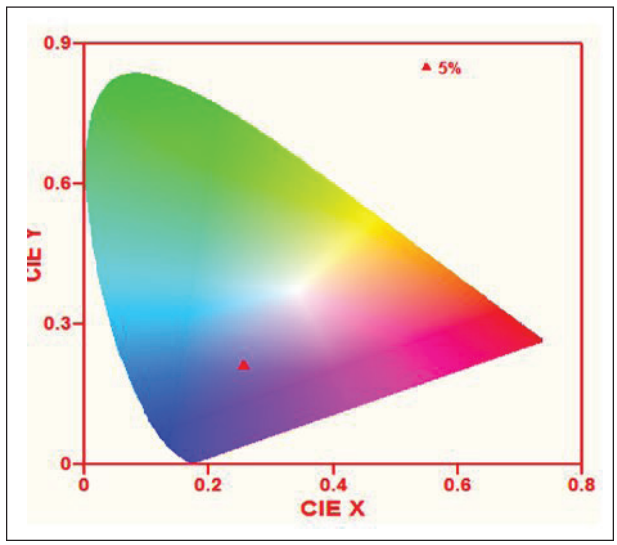

Fig. 6: CIE Chromaticity Diagram for as Prepared Sample of $CdMoO_4:Pr^{3+}$(5 at. %).

Lifetime Study

At room temperature, the produced samples of $CdMoO_4:Pr^{3+}$(5 at. %) measured with the excitation fixed at 468 nm exhibit decay curves depicted in Fig. 7, displaying the typical bi-exponential fitting for the same sample. The samples' fit (R^2) qualities for the concentrations was 0.97773 respectively, and the estimated average lifetimes is 5.08835, respectively. The bi-exponential equation can be used to fit all decay curves effectively:

$$I = I_1 \exp(-t/T_1) + I_2 \exp(-t/T_2)$$

where I_1 and I_2 stand for intensities at time '0' and 't,' and 1 and 2 are the times at which they would decay, respectively. An activator's bi-exponential decay pattern suggests the existence of Pr^{3+} in two separate sites and is frequently linked to the transmission of excitation energy from the donor. A particle with a spherical form has two sites: an inner core and a surface site. Because the impurities and surface flaws on the sample's surface may serve as pathways for non-radiative relaxation, the Pr^{3+} at surface sites should have a shorter projected lifetime. In contrast, the Pr^{3+} at inner core sites should have a longer predicted lifetime (Singh *et al*. 2020). Using the formula shown below, one can determine the average lifetime:

$$\tau_{ave} = I_1 T^2_1 + I_2 T^2_2 / I_1 T_1 + I_2 T_2$$

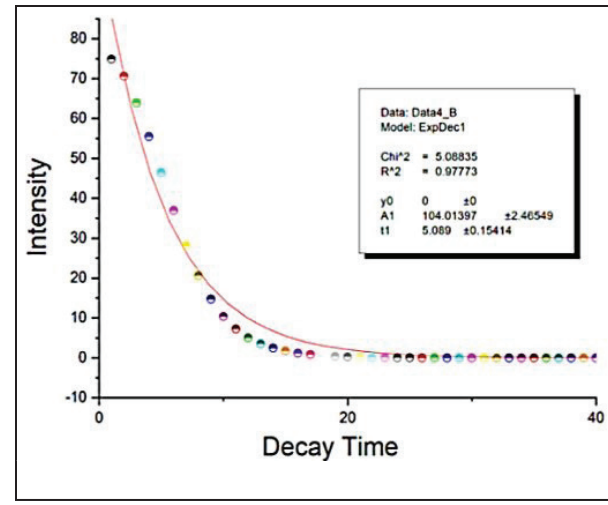

Fig. 7: Photoluminescence Decay Curve of $CdMoO_4:Pr^{3+}$.

PHOTOCATALYTIC STUDY

Methyl Red was used as the target pollutant to evaluate the photocatalytic activity of the produced materials under 50-watt LED Philips Stellar irradiation. Under 50-watt LED Philips Stellar irradiation, Fig. 8 illustrates the degradation efficiency of methyl red using $CdMoO_4$ photocatalysts produced in distilled water, respectively. Without the catalyst, photo-induced dye self-degradation was essentially non-existent. However, when the catalyst was present, a notable deterioration was seen (Singh *et al*. 2020). This finding suggests that $CdMoO_4$ may work well as a visible light active photocatalyst to degrade methyl red dye. After 150 minutes of exposure to a 50-watt LED Philips Stellar, the $CdMoO_4$ photocatalyst that was prepared was able to degrade 95.063% of the Methyl Red dye, while the $CdMoO_4$ photocatalyst that was prepared with water only degraded 73.244% of the dye in 60 minutes. Because of their short band-gap energy, $CdMoO_4$ photocatalysts are readily photoexcited by 50-watt LED Philips Stellar irradiation. When exposed to sunlight, an electron in the valence band is stimulated to the conduction band, creating an electron-hole pair and a hole in the valence band. O_2 was adsorbed from water molecules by the electron in the conduction band of the $CdMoO_4$ photocatalyst, creating $O^{2-\cdot}$. Conversely, the valence band hole forms $OH\cdot$ through interactions with adsorbed water molecules. Methyl Red dye breaks down into carbon dioxide and water under the influence of $O^{2-\cdot}$ and $OH^{\cdot}$. This discovery concludes that the catalyst's photocatalytic activity is significantly influenced by the solvents utilised in the synthesis.

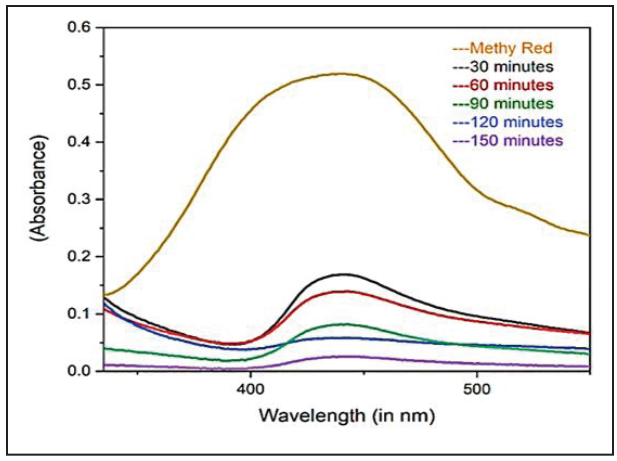

Fig. 8: Degradation of $CdMoO_4:Pr^{3+}$.

KINETIC STUDY

The kinetics of Methyl Red degradation under 50-watt Philips Stellar LED illumination was addressed. The graphs between ln [C_t] vs time (Fig. 9) was plot using the equation:

$$\ln(C_o/C_t)=k_t$$

showed first-order kinetics having an R^2 value of 0.977, where C_t stand for Methyl Red's initial and time-at-time concentrations, respectively (Singh *et al*. 2020).

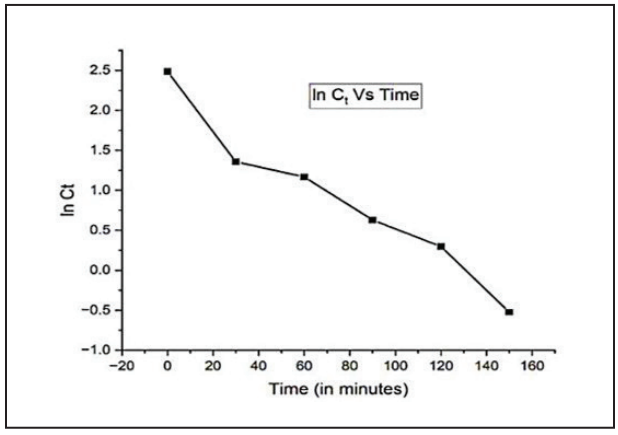

Fig. 9: Kinetic Rate of Degradation of Methyl Red Using Prepared $CdMoO_4:Pr^{3+}$.

CONCLUSION

$CdMoO_4:Pr^{3+}$, the host of the rare-earth-doped luminous nanoparticle we obtained, was successfully doped. Cell parameters (JCPDS no. 07-0209) are a = b = 5.155, c = 11.194, and V = 297.473; our as-prepared sample is a tetragonal structure of $CdMoO_4$ with a bluish-purple hue in the CIE diagram, as is evident from the data acquired from the absorption spectra, the Fourier transform infrared area, the XRD diagram, and luminescence spectroscopy. The image of the sample is also examined with the scanning electron microscope (SEM), where we can see its morphology, but it is not well portrayed due to agglomeration.

For photocatalytic degradation, methyl red was added to the synthesis of $CdMoO_4:Pr^{3+}$ and was degraded under Philip LED light at 30, 60, 90, 120 and 150 min intervals of time. The degradation decreases with increases in time, and the photocatalytic efficiency of $CdWO_4$ was calculated using the formula: Degradation efficiency% = $[C_0\text{-}C_t]/C_0 \times 100$ and obtained about 95.063%, a remarkably high efficiency. The bi-exponential equation can be used to fit the decay curves with good accuracy for our prepared sample obtaining a R^2 value of 0.977, indicating that the process will follow first-order kinetics.

ACKNOWLEDGEMENT

The authors express their gratitude to the Department of Chemistry, School of Physical Sciences, DST-Funding, Mizoram University, Aizawl, Mizoram, for providing the advanced instrumentation equipment necessary to meet our requirements.

REFERENCES

Gai S., Li C., Yang P., & Lin J. (2014). Recent Progress in Rare Earth Micro/Nanocrystals: Soft Chemical Synthesis, Luminescent Properties, and Biomedical Applications. *Chemical Reviews,* 114(4), 2343–2389. https://doi.org/10.1021/cr4001594

Wang D., Fan J., Shang M., Li K., Zhang Y., Lian H., & Lin J. (2016). Pechini-type sol-gel synthesis and multicolour-tunable emission properties of $GdY(MoO_4)_3:RE^{3+}$ (RE=Eu, Dy, Sm, Tb) phosphors. *Optical Materials, 51*, 162–170. https://doi.org/10.1016/j.optmat.2015.11.029

Vranješ M., Kuljanin-Jakovljević J., Ahrenkiel S. P., Zeković I., Mitrić M., Šaponjić Z., & Nedeljković J. M. (2013). Sm^{3+} doped TiO_2 nanoparticles synthesized from nanotubular precursors—Luminescent and structural properties. *Journal of Luminescence, 143*, 453–458. https://doi.org/10.1016/j.jlumin.2013.05.022

Lin J., Zeng Z., & Wang Q. (2013). $CdMoO_4:Eu^{3+}$ micro-sized luminescent particle synthesis and photocatalytic performance. *Inorganica Chimica Acta, 408*, 59–63. https://doi.org/10.1016/j.ica.2013.08.023

Wang W. S., Zhen L., Xu C. Y., Shao W. Z., & Chen Z. L. (2012). Eu^{3+}-doped $CdMoO_4$ red phosphor synthesized through an aqueous solution route at room temperature. *Journal of Alloys and Compounds*, *529*, 17–20. https://doi.org/10.1016/j.jallcom.2012.03.058

Zhang J., Zhang N., Zou L., & Gan S. (2014). Formation mechanism and optical properties of $CdMoO_4$ and $CdMoO_4:Ln^{3+}$ (Ln = Pr, Sm, Eu, Dy, Ho and Er) microspheres synthesized via a facile sonochemical route. *RSC Advances*, *4*(72), 38455–38465. https://doi.org/10.1039/C4RA05038J

Singh N. P., Singh N. R., & Singh N. M. (2018). Synthesis of $CdMoO_4:Sm^{3+}$ phosphors at room temperature and investigation of photoluminescence properties. *Optik*, *156*, 365–373. https://doi.org/10.1016/j.ijleo.2017.11.045

Longo V. M., Cavalcante L. S., Paris E. C., Sczancoski J. C., Pizani P. S., Li M. S., Andrés J., Longo E., & Varela J. A. (2011). Hierarchical Assembly of $CaMoO_4$ Nano-Octahedrons and Their Photoluminescence Properties. The *Journal of Physical Chemistry C*, *115*(13), 5207–5219. https://doi.org/10.1021/jp1082328

Liu X., Lv L., Huang S., Su Y., & Wang X. (2014). Microwave-assisted synthesis and luminescence properties of $Cd(1-x)Eu(x)MoO_4$ red phosphor. *Journal of Nanoscience and Nanotechnology*, *14*(5), 3618–3622. https://doi.org/10.1166/jnn.2014.7992

Yang X., Zhou Y., Yu X., Demir H. V., & Sun X. W. (2011). Bifunctional highly fluorescent hollow porous microspheres made of $BaMoO_4:Pr^{3+}$ nanocrystals via a template-free synthesis. *Journal of Materials Chemistry*, *21*(25), 9009–9013. https://doi.org/10.1039/C1JM10458F

Sharma K., Singh D. T., & Nongmaithem R. (2014). Low-temperature synthesis, characterization and tunable optical properties of Eu^{3+}, Tb^{3+} doped $CaMoO_4$ nanoparticles. *Journal of Alloys and Compounds*, *602*, 275–280. https://doi.org/10.1016/j.jallcom.2014.02.186

Singh N. P., Singh N. R., Devi Y. R., Singh Sh B., Singh Th. D., Singh N. R., & Singh N. M. (2020). Effects of annealing temperature on structural and luminescence properties of $CdMoO_4:Dy^{3+}$ phosphor synthesized at room temperature by co-precipitation method. *Solid State Sciences, 102*, 106172. https://doi.org/10.1016/j.solidstatesciences.2020.106172

Naorem R. S., Singh N. P., & Singh N. M. (2020). Photoluminescence studies of Ce^{3+} ion-doped $BiPO_4$ phosphor and its photocatalytic activity. *International Journal of Applied Ceramic Technology*, *17*(6), 2744–2751. https://doi.org/10.1111/ijac.13600

Singh N. M., Naorem R. S., Lalthlamuanpuii H., Lalhmingmawia, & Borgohain, D. (2020). Kinetic study for the interaction of Nd(III) with creatine in different organic solvents using 4f-4f transition spectra as a probe. *Journal of the Indian Chemical Society*, *97*(11b), 2385–2390.